Mechanism of Ba^{2+} block of a mouse inwardly rectifying K^+ channel: differential contribution by two discrete residues

Noga Alagem, Miri Dvir and Eitan Reuveny

Department of Biological Chemistry, Weizmann Institute of Science, Rehovot 76100, Israel

(Received 23 November 2000; accepted after revision 12 March 2001)

1. The block of the IRK1/Kir2.1 inwardly rectifying K^+ channel by a Ba^{2+} ion is highly voltage dependent, where the ion binds approximately half-way within the membrane electrical field. The mechanism by which two distinct mutations, E125N and T141A, affect Ba^{2+} block of Kir2.1 was investigated using heterologous expression in *Xenopus* oocytes.

2. Analysis of the blocking kinetics showed that E125 and T141 affect the entry and binding of Ba^{2+} to the channel, respectively. Replacing the glutamate at position 125 with an asparagine greatly decreased the rate at which the Ba^{2+} ions enter and leave the pore. In contrast, replacing the polar threonine at position 141 with an alanine affected the entry rate of the Ba^{2+} ions while leaving the exit rate unchanged.

3. Acidification of the extracellular solution slowed the exit rate of the Ba^{2+} from the wild-type channel, but had no such effect on the Kir2.1(E125N) mutant.

4. These results thus reveal two unique roles for the amino acids at positions 125 and 141 in aiding the interaction of Ba^{2+} with the channel. Their possible roles in K^+ permeation are discussed.

Inwardly rectifying potassium (Kir) channels are involved in many physiological processes, such as setting the excitability state of nerve and muscle, potassium secretion and hormone release. They act by allowing the flux of potassium ions near the potassium equilibrium potential, thus keeping the resting membrane potential hyperpolarized. The inward rectification is attributed to a voltage-dependent block of the channel pore by intracellular magnesium and polyamines (Fakler *et al.* 1995; Lopatin *et al.* 1995).

Inorganic cations have been widely used to probe the permeation and gating mechanisms of potassium channels (Hille, 1992). Inwardly rectifying potassium channels display a particularly high affinity for various monovalent and divalent cations. Kir channel block by external monovalent cations, namely protons, Na^+, Cs^+, Rb^+ and Ag^+, or by divalent cations, such as Ba^{2+}, Mg^{2+}, Ca^{2+} and Sr^{2+}, has been studied in native tissues, as well as in cloned channels expressed in various heterologous systems (Standen & Stanfield, 1978, 1980; Ohmori, 1978; Biermans *et al.* 1987; Harvey & Ten Eick, 1989; Shioya *et al.* 1993; Reuveny *et al.* 1996; Sabirov *et al.* 1997*a*; Shieh *et al.* 1998; Doring *et al.* 1998; Dart *et al.* 1998). The interaction of divalent cations with Kir channels is thought to occur via two distinct binding sites; a shallow site that barely senses the membrane electric field, and a deeper one located approximately half-way within the membrane electrical field. Channel block by Mg^{2+} and Ca^{2+} ions was found to occur through the shallow site, whereas the block by Ba^{2+} and Sr^{2+} ions is mediated through the deeper one (Standen & Stanfield, 1978; Shioya *et al.* 1993; Reuveny *et al.* 1996; Sabirov *et al.* 1997*b*; Shieh *et al.* 1998). For all divalent cations, a single ion suffices to block the channel. In most cases of deep-site blockers, the block follows first-order kinetics, taking several seconds to reach a steady-state (Standen & Stanfield, 1978; Shieh *et al.* 1998). An exception is the G-protein-coupled inwardly rectifying potassium channel family, where part of the Ba^{2+} block reaches steady state in an unmeasurably short time (Carmeliet & Mubagwa, 1986).

Since the recent cloning of many Kir channels, some progress has been made in understanding the molecular mechanisms involved in the channel block by divalent cations. Sabirov *et al.* (1997*b*) showed that a highly conserved arginine residue at position 148 in Kir2.1/IRK1 forms a barrier for external cations. Mutating R148 to histidine allowed Mg^{2+} and Ca^{2+} (shallow blockers) to bind more deeply within the electric field. Block by Ba^{2+} and Cs^+ became more rapid, while the affinity and voltage dependence of the block remained unchanged. Additional information related to the role of this conserved arginine in channel block came from a unique member of the Kir channel family, Kir7.1. This channel has a methionine at the position corresponding to that of the conserved arginine. This methionine was

found to account for the unique permeation properties exhibited by Kir7.1, including a very low affinity for Ba^{2+} (Doring *et al.* 1998; Krapivinsky *et al.* 1998). Other sites in Kir channels have been found to affect the Ba^{2+} block. For example, Zhou *et al.* (1996) showed that in Kir1.2/ROMK2, a single mutation at position 121 from valine to threonine (the corresponding residue in Kir2.1), rendered the channel more sensitive to Ba^{2+} block. In addition, the presence of a glutamate at position 125 in Kir2.1 was shown to affect Ba^{2+} sensitivity as well as the single-channel conductance. The Ba^{2+} sensitivity of cKir2.1, cloned from chick inner ear, was increased 6-fold by mutating the asparagine at position 125 to glutamate, the corresponding residue in human and in mouse Kir2.1 (Navaratnam *et al.* 1995). Finally, Kir2.4/IRK4, which has a glutamine at the 125 position, also has a reduced affinity for Ba^{2+} and a smaller single-channel conductance (Topert *et al.* 1998). Despite all this information regarding the structural elements affecting Ba^{2+} block, the mechanism by which all these identified residues contribute to this process is still unclear.

In the light of the recent elucidation of the three-dimensional structure of the KcsA bacterial K^+ channel, and its topological similarity to Kir channels, it seems that the residues that affect the Ba^{2+} block are located at rather distinct regions. In the present work we studied the mechanism by which E125, located at the outer channel vestibule, and T141, located close to the selectivity filter, control the affinity of Kir2.1 for Ba^{2+}. The voltage dependence of block as well as the blocking kinetics were measured in the mutant channels, and were compared to those of the wild-type Kir2.1. Our results suggest two distinct roles of the two sites in channel block by Ba^{2+} and in K^+ permeation.

METHODS

Mutagenesis

Mutations of the mouse *Kir2.1* gene were introduced by standard two-step PCR, using an oligonucleotide that carries a silent restriction site next to the desired mutation for screening purposes. The PCR products were then subcloned back into the parental gene, using silent restriction sites that were previously engineered into the mouse *Kir2.1* gene (Kubo *et al.* 1993). Positive clones were verified by sequencing of the relevant subcloned fragment.

RNA preparation

Capped cRNA was transcribed using a home-assembled cRNA transcription kit (Stratagene and Pharmacia). The cRNA integrity and concentration were determined by running an aliquot on a formaldehyde gel.

Solutions

ND96 solution contained (mM): 96 NaCl, 2 KCl, 1 $CaCl_2$, 1 $MgCl_2$ and 5 Hepes, pH 7.4. Nominally calcium-free ND96 solution was prepared as above, but without $CaCl_2$. For two-electrode voltage-clamp (TEVC) recordings, the bath solution, which will be referred to as 90K solution, contained (mM): 90 KCl, 10 Hepes and 2 $MgCl_2$, pH 7.4 (KOH). In some of the experiments, the pH of the 90K solution was brought to pH 4.0 by adding HCl. The 10 mM KCl solution used for some of the unblocking measurements contained (mM): 10 KCl, 87 NMDG (*N*-methyl-D-glucamine), 10 Hepes and 2 $MgCl_2$, pH 7.4 (HCl). $BaCl_2$ diluted from a 1 M stock was added to the various solutions as indicated. In some cases, 100 μM niflumic acid (Sigma Chemical Co.) was freshly added to the external solutions in order to block the oocyte's endogenous gap junction channels (Zhang *et al.* 1998). For patch-clamp recordings, both the pipette and the bath solution contained 90K. When necessary, the patch pipette also contained 50 μM $GdCl_3$, aimed at blocking the endogenous mechano-sensitive channels (Yang & Sachs, 1989). Neither 100 μM niflumic acid nor 50 μM $GdCl_3$ block Kir2.1 to a measurable extent.

Oocyte preparation

Female *Xenopus laevis* frogs were handled according to the guidelines of the Weizmann Institute of Science. Ovarian lobes were removed from the frogs under 0.15 % (w/v) tricaine (Sigma Chemical Co.) anaesthesia. Frogs were humanely killed after the final collection. Oocytes were defolliculated by shaking in Ca^{2+}-free ND96 solution containing 2 mg ml^{-1} Type 1 collagenase (Worthington) for ~1 h at room temperature. The oocytes were then washed in ND96 solution. Healthy stage 5–6 oocytes were selected, and then micro-injected with 50 nl cRNA of the various channel mutants.

TEVC

Currents through the expressed channels were recorded by the TEVC technique using a CA1-B amplifier (Dagan Corp.) (Reuveny *et al.* 1994). Electrodes were filled with 3 M KCl and had a resistance of 0.1–0.6 MΩ. Data acquisition and analysis were done using the pCLAMP 6.04 software package (Axon Instruments). Only oocytes that expressed currents of less than 12 μA at −100 mV were used in the experiments due to an apparent decrease in the affinity for Ba^{2+} at higher channel densities (N. Alagem & E. Reuveny, unpublished observation; see also Navaratnam *et al.* 1995). It should be mentioned that the manner by which the level of expressed current affects the Ba^{2+} sensitivity is not yet understood. However, similar phenomena have been reported in voltage-gated K^+ channels expressed in *Xenopus* oocytes as well as in other heterologous systems. It has been suggested that the effect of expression levels on current characteristics may result from channel clustering, some erroneous post-translational modification or the accumulation of K^+ close to the membrane (Moran *et al.* 1992; Honore *et al.* 1992; Grigoriev *et al.* 1999). Oocytes were held at 0 mV unless otherwise indicated and voltage steps from +30 to −120 mV in 10 mV decrements were applied, each for 4 s. Between pulses, the membrane was held at 0 mV for at least 6 s, allowing the channel to recover from the block. For blocking kinetics measurements in Kir2.1(E125N) and Kir2.1(E125Q), the holding potential was +30 mV, the duration between pulses was 20 s and the pulse duration was 5 s. For steady-state blocking measurements in Kir2.1(E125N–T141A) the holding potential was +30 mV, the duration between pulses was 20 s and the pulse duration was 6.5 s. Solutions were changed using a gravitational flow system. The oocyte was washed for at least 30 s with each solution prior to data recording. This, apparently, was sufficient to equilibrate the system, as more prolonged washing did not produce further blocking. For unblocking experiments, an oocyte was placed in the 90K solution containing 100 μM $BaCl_2$ (wild-type Kir2.1 and Kir2.1(E125D)) or 300 μM $BaCl_2$ (Kir2.1(T141A), Kir2.1(E125Q) and Kir2.1(E125N)).

Patch clamp

Single-channel currents were measured by the patch-clamp technique (Hamill *et al.* 1981) in the cell-attached mode, using an Axopatch 200B amplifier (Axon Instruments). Current traces were low-pass filtered at 5 kHz, digitized at 94.4 kHz (VR-10B analog-to-

digital converter, Instrutech), and stored on a VCR tape. For analysis, data segments of interest were low-pass filtered at 1 kHz using an 8-pole Bessel filter (Frequency Devices), digitized at 5 kHz using Digidata 1200B (Axon Instruments), stored on a computer hard disk, and analysed using pCLAMP version 6.04.

Data manipulation

The blocking time constants were calculated using Clampfit (pCLAMP 6.04). All other curve-fitting procedures were performed using Sigma Plot 4.0. All measurements were collected from at least two different batches, $n = 3$–7 oocytes. Data are presented as means ± standard error of the mean (S.E.M.). Results that were extracted from a curve-fit are presented as the fitted value ± standard deviation (S.D.) of the fit. Statistical significance was tested using one-way ANOVA. The significance of the difference was set at $P < 0.05$.

RESULTS

Steady-state block by extracellular Ba^{2+}

Ba^{2+} ions produced a time- and voltage-dependent block in wild-type Kir2.1 and the two mutants Kir2.1(T141A) and Kir2.1(E125N). Figure 1*A* shows typical steady-state current *vs.* voltage plots at different concentrations of extracellular Ba^{2+}. The steady-state current level was measured at the end of a 4 s-long voltage step for each potential. We verified that the current level at the end of the pulse was sufficiently close to steady-state in two ways. First, in one batch of Kir2.1(E125N)-injected oocytes, the voltage steps were applied for 5 s, and the dose–response was calculated. The affinity in this case was similar to that calculated by using the 4 s-long pulses (data not shown). Second, analysis of the voltage dependence of the dissociation constant (K_d) did not show any apparent over-estimation of K_d at relatively positive potentials (Fig. 2*B*). The unblocked fractional current I_f was calculated as:

$$I_f = \frac{I_{ss}(Ba^{2+})}{I_{ss}(90K)}, \quad (1)$$

where $I_{ss}(Ba^{2+})$ is the leak-subtracted steady-state current recorded for each Ba^{2+} concentration and $I_{ss}(90K)$ is the

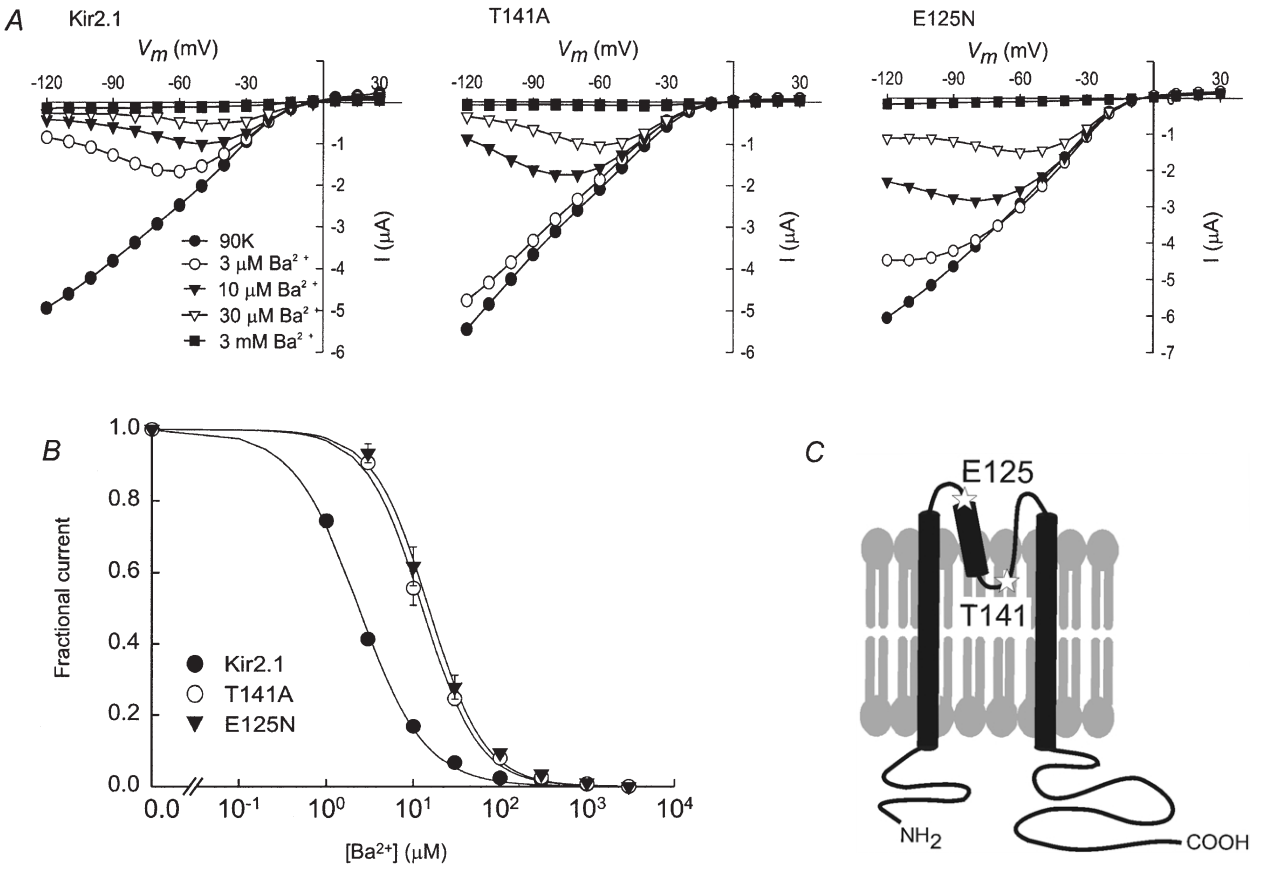

Figure 1. Steady-state Ba^{2+} block of Kir2.1 and the two mutants Kir2.1(T141A) and Kir2.1(E125N)

A, typical steady-state current *vs.* voltage plots measured for one representative oocyte in the presence of 90K with varying concentrations of extracellular Ba^{2+} for Kir2.1 (left), Kir2.1(T141A) (centre) and Kir2.1(E125N) (right). *B*, fractional current *vs.* Ba^{2+} concentration at steady state, at a holding potential of −80 mV. The smooth lines are fits to the Hill equation (eqn (2)). *C*, a simplified two-dimensional cartoon showing the approximate positions of E125 and T141 (stars) in the Kir2.1 channel.

leak-subtracted steady-state current recorded without Ba^{2+}. The steady-state current recorded in 90K containing 3 or 10 mM Ba^{2+} was used as the leak current. In Fig. 1*B* the unblocked fractional current was plotted as a function of the Ba^{2+} concentration for the wild-type channel and the two mutants. The resulting curves were sigmoidal, and each could be fitted by the Hill equation:

$$I_f = \frac{K_d^{n_H}}{K_d^{n_H} + [Ba^{2+}]^{n_H}}, \quad (2)$$

where n_H is the Hill coefficient and $[Ba^{2+}]$ is the Ba^{2+} molar concentration. Kir2.1 was half-blocked at 2.7 ± 0.1 μM Ba^{2+} ($n_H = 1.14 \pm 0.04$) at −80 mV. This result is in good agreement with the value of 2.2 μM at −80 mV measured by Shieh *et al.* (1998). Kir2.1(E125N) and Kir2.1(T141A) had lower affinities for Ba^{2+}, with K_d values of 15.6 ± 0.5 μM ($n_H = 1.41 \pm 0.06$) and 12.7 ± 0.6 μM Ba^{2+} ($n_H = 1.34 \pm 0.07$), respectively.

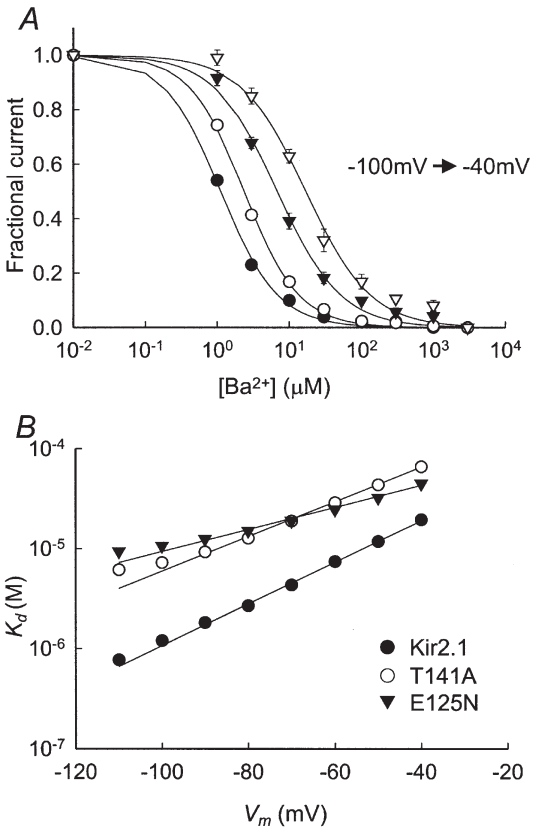

Figure 2. Voltage dependence of the steady-state Ba^{2+} block

A, Ba^{2+} concentration dependence of the steady-state block of Kir2.1 at different holding potentials (−100 to −40 mV, indicated by different symbols) in 20 mV increments. The data points at −80 mV are the same as in Fig. 1*B*. The smooth lines are fits to the Hill equation (eqn (2)). *B*, voltage dependence of K_d. The smooth lines are fits to eqn (3).

Voltage dependence of the steady-state block

Although the E125N and T141A mutations influence the Ba^{2+} affinity to a similar extent, it is likely that the mechanisms are different, as T141 and E125 are located in different regions of the Kir2.1 channel (Fig. 1*C*). To determine whether the voltage dependence of block had changed in either of the mutants, we analysed the blocking affinity at various potentials.

As expected for a deep-site blocker, the block was highly voltage dependent, both in the wild-type channel and in the two mutants (Fig. 2). According to Woodhull's model (Woodhull, 1973) the voltage dependence of the dissociation constant would be given by:

$$K_d(V) = K_d(0)\exp\left(\frac{zF\delta}{RT}V\right), \quad (3)$$

where $K_d(0)$ is the dissociation constant at zero voltage, z is the ion valency, F is the Faraday constant, δ is the fractional potential drop at the binding site (often referred to as electrical distance), V is the membrane potential, R is the gas constant and T is the absolute temperature. A fit of our results to eqn (3) yielded $K_d(0) = 131 \pm 7$ μM for Kir2.1, 134 ± 9 μM for Kir2.1(E125N) and 320 ± 18 μM for Kir2.1(T141A). While there was no significant difference between $K_d(0)$ of the wild-type and the Kir2.1(E125N) mutant, $K_d(0)$ of the Kir2.1(T141A) mutant was significantly higher than that of the wild-type. The electrical distances, δ, that were obtained from the fit were 0.62 ± 0.01 for Kir2.1, 0.34 ± 0.02 for Kir2.1(E125N) and 0.51 ± 0.01 for Kir2.1(T141A).

Block kinetics

A mutation could lower the Ba^{2+} affinity by decreasing the blocking rate, or alternatively by increasing the unblocking rate, or by both methods. Therefore, the effects of the two mutations on the blocking and the unblocking rates of the reaction were characterized. Figure 3*A–D* shows current traces elicited in response to voltage steps ranging from +30 to −120 mV in 10 mV decrements. The currents in Fig. 3*B–D* were recorded in 90K containing 10 μM Ba^{2+}. The time required for the blocking reaction to reach steady state was longer in Kir2.1(T141A) and in Kir2.1(E125N), compared to that required for the wild-type channel. The blocking time constant was calculated by fitting the currents to an exponentially decaying function of the form:

$$I = A\exp(-t/\tau_{block}) + C, \quad (4)$$

where A is the current amplitude, t is time measured from the pulse onset, τ_{block} is the blocking time constant and C is the steady-state current. The voltage dependence of the blocking time constants is shown in Fig. 3*E*. The blocking time constants for the wild-type and the mutant channels increased exponentially with depolarization. The blocking time constant increased e-fold per 33.9 ± 1.0,

40.6 ± 1.6 and 38.2 ± 0.8 mV of depolarization for Kir2.1, Kir2.1(T141A) and Kir2.1(E125N), respectively.

Assuming that steady-state blocking is a result of a dynamic equilibrium between blocking and unblocking processes, the blocking time constant may be expressed as

$$\tau_{\text{block}} = \frac{1}{k_{\text{on}}[\text{Ba}^{2+}] + k_{\text{off}}}, \quad (5)$$

where k_{on} is the blocking rate coefficient and k_{off} is the unblocking rate coefficient. Experimentally, plotting the blocking rate, which is the reciprocal of the blocking time constant, as a function of Ba^{2+} concentration, yields the values of k_{on} and k_{off} as the slope and y-axis intercept, respectively (Fig. 4*A–C*). In Fig. 4*D* the blocking rates are plotted as functions of the membrane potential. The curve was fitted by a modified form of eqn (3), in which $k_{\text{on}}(V)$ was substituted for $K_{\text{d}}(V)$, $k_{\text{on}}(0)$ was substituted for $K_{\text{d}}(0)$ and δ_{on} (the electrical distance between the entrance of the channel pore and the energy barrier) was substituted for δ (Reuveny *et al.* 1996):

$$k_{\text{on}}(V) = k_{\text{on}}(0)\exp\left(-\frac{zF\delta_{\text{on}}}{RT}V\right). \quad (6)$$

The fit yielded the following values of $k_{\text{on}}(0)$ and δ_{on}. Kir2.1: $k_{\text{on}}(0) = 29.4\,(\pm 3.4) \times 10^3\ \text{s}^{-1}\ \text{M}^{-1}$, $\delta_{\text{on}} = 0.28 \pm 0.01$; Kir2.1(E125N): $2.2\,(\pm 0.2) \times 10^3\ \text{s}^{-1}\ \text{M}^{-1}$, $\delta_{\text{on}} = 0.32 \pm 0.01$; Kir2.1(T141A): $5.1\,(\pm 0.3) \times 10^3\ \text{s}^{-1}\ \text{M}^{-1}$, $\delta_{\text{on}} = 0.36 \pm 0.01$. In Fig. 4*E* the unblocking rates of Kir2.1 and the two mutants are plotted as a function of the membrane potential. Between −40 mV and −90 mV the k_{off} values of wild-type Kir2.1 and the Kir2.1(T141A) mutant gradually decrease as the membrane potential becomes more hyperpolarized. At membrane potentials that are more negative than −100 mV, the k_{off} values start to increase exponentially. The unblocking rate of Kir2.1(E125N), however, does not exhibit this biphasic relationship with voltage observed for the wild-type and

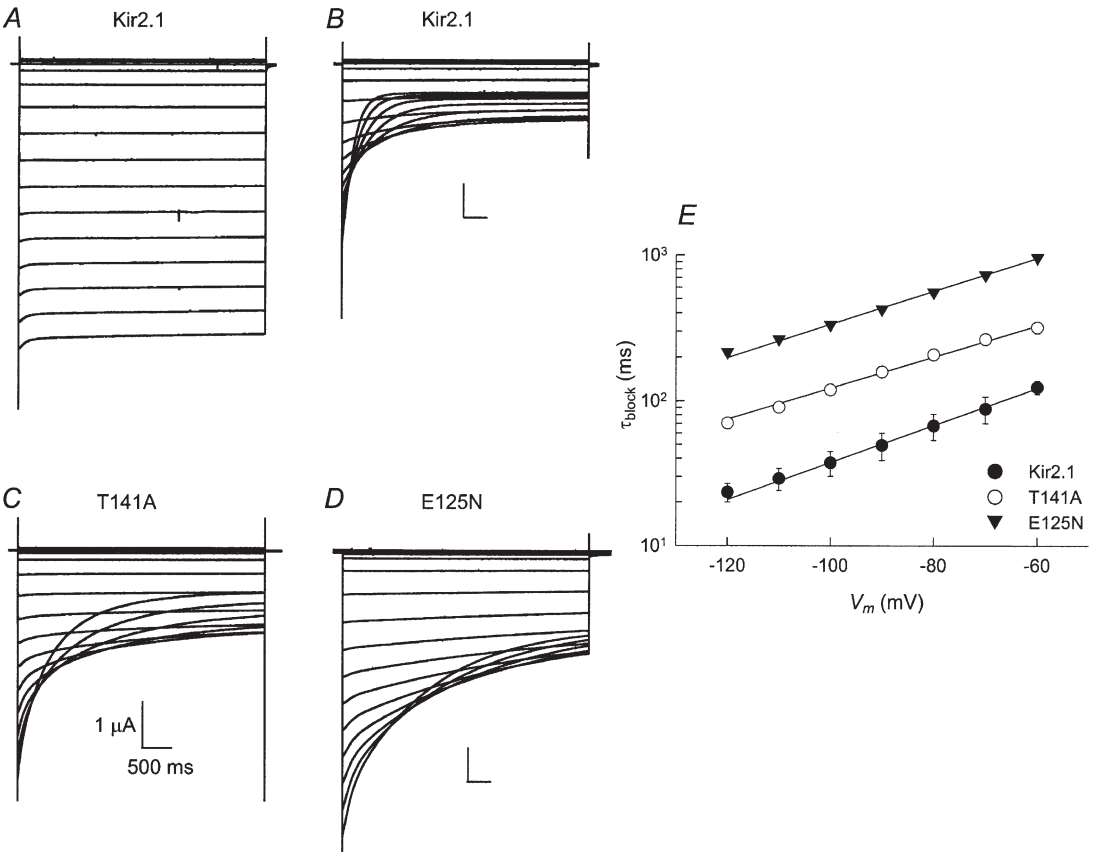

Figure 3. Time dependence of Ba^{2+} block of the Kir2.1 channel and the Kir2.1(T141A) and Kir2.1(E125N) mutants

A–D, current traces elicited by voltage steps ranging from +30 to −120 mV in 10 mV decrements. Each family of traces was recorded from a representative oocyte expressing Kir2.1, Kir2.1(E125N) or Kir2.1(T141A) channels. The bath solution contained 90K (*A*) or 90K and 10 μM Ba^{2+} (*B–D*). The Kir2.1 currents shown in *A* and *B* were recorded from the same oocyte. *E*, voltage dependence of the blocking time constant. The data points were obtained in the presence of 100 μM Ba^{2+}.

the Kir2.1(T141A) mutant channels. Instead, the unblocking rate steadily increases as the membrane potential becomes more hyperpolarized. The increase in k_{off} at very negative potentials has been noticed previously in Kir2.1, as well as in voltage-gated K^+ channels and in BK channels, and was attributed to the dissociation of Ba^{2+} ions to the intracellular solution (Neyton & Miller, 1988*b*; Harris *et al.* 1998; Shieh *et al.* 1998). The k_{off}/k_{on} ratios were compared with the K_d values extracted from the steady-state current levels. The values were similar: at −80 mV $K_d = 2.7 \pm 0.1$ μM and $k_{off}/k_{on} = 2.0 \pm 0.2$ μM for wild-type Kir2.1.

Recovery from block at positive potentials

It was of interest to see whether the differences in the unblocking rates among Kir2.1 and the two mutants, measured at negative potentials, were also reflected under positive potentials, where the exit rate of Ba^{2+} is dominant. A double-pulse protocol was applied to measure k_{off} at positive potentials: Ba^{2+} block was initiated by a hyperpolarizing control step to −100 mV for 1.2 s in duration. A step to a test depolarizing potential was applied for various durations, allowing a fraction of the channels to recover from the block, followed by a second hyperpolarizing step to −100 mV (Fig. 5*A*). The ratio of the instantaneous current elicited by the second pulse to the instantaneous current elicited by the control pulse, which reflects the recovery of the channel from block, was calculated using:

$$\mathrm{FR} = \frac{I_{\mathrm{inst(second\ pulse)}} - I_{\mathrm{ss(second\ pulse)}}}{I_{\mathrm{inst(control\ pulse)}} - I_{\mathrm{ss(control\ pulse)}}}, \quad (7)$$

where FR is the fractional current recovery, I_{inst} is the instantaneous current elicited by each hyperpolarizing step and I_{ss} is the current level at steady state. Since the recovery measurements were conducted at Ba^{2+} concentrations sufficient to produce full block at steady state (100 μM for Kir2.1, 300 μM for Kir2.1(E125N) and Kir2.1(T141A)), I_{ss} is mainly the leak current. Kir2.1 and Kir2.1(E125N) channel recovery from Ba^{2+} block could be described as a mono-exponential function:

$$\mathrm{FR}(t) = \mathrm{FR}_{max}(1 - \exp(-t/\tau_{recovery})), \quad (8)$$

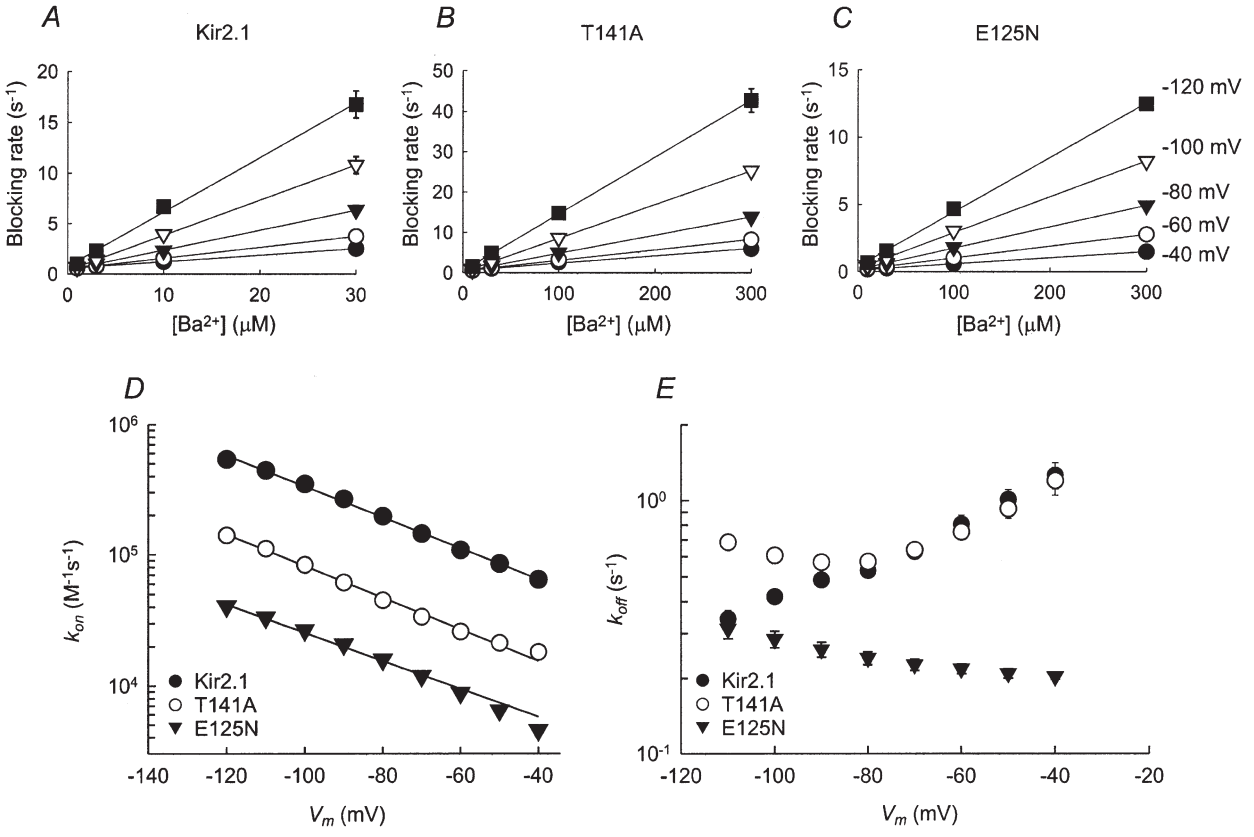

Figure 4. Voltage dependence of Ba^{2+} blocking kinetics

A–C, the blocking rate (the reciprocal of the blocking time constant, τ_{block}) as a function of the extracellular Ba^{2+} concentration at various membrane potentials. The continuous lines are linear regressions. *D*, voltage dependence of the blocking rate constants (k_{on}). Data points are the slopes of the linear regression as shown in *A–C*. The error bars are the standard deviation of the fit (where error bars are not visible, they are smaller than the symbols). Continuous lines are fits to eqn (6). *E*, voltage dependence of the unblocking rate constant (k_{off}). Data points were obtained by multiplying K_d by k_{on} for each voltage.

where FR_{max} is the maximal fractional recovery, t is time and $\tau_{recovery}$ is the time constant for current recovery. The experimental time constants were 0.70 ± 0.02 s for Kir2.1 and 2.00 ± 0.05 s for Kir2.1(E125N) channels at +60 mV. The recovery of Kir2.1(T141A), however, could only be fitted to a bi-exponential function:

$$FR(t) = FR_{max,1}(1 - \exp(-t/\tau_{slow})) + FR_{max,2}(1 - \exp(-t/\tau_{fast})), \quad (9)$$

with time constants of 0.03 ± 0.001 s (40 %) and 0.84 ± 0.02 s (60 %) at +60 mV. Figure 5*B* shows that while the slow component of Kir2.1(T141A) was similar to that of Kir2.1, the unblocking rate of Kir2.1(E125N) was considerably slower. The existence of two components for the Ba^{2+} unblocking time course of the Kir2.1(T141A) mutant suggests that this process may be mediated by two kinetically distinct steps. The structural basis for this phenomenon is not known at the moment, but may be due to the non-polar nature of the alanine residue in the 141 position, or to the uncovering of an intermediate binding site once the polar threonine is replaced.

The voltage dependence of the unblocking rate was analysed, using a modified form of eqn (3):

$$k_{off}(V) = k_{off}(0)\exp\left(-\frac{zF\delta_{off}}{RT}V\right). \quad (10)$$

The following values of $k_{off}(0)$ and δ_{off} were obtained. WT Kir2.1: $k_{off}(0) = 0.66 \pm 0.07\ s^{-1}$, $\delta_{off} = 0.18 \pm 0.02$; Kir2.1(E125N): $k_{off}(0) = 0.29 \pm 0.04\ s^{-1}$, $\delta_{off} = 0.09 \pm 0.02$;

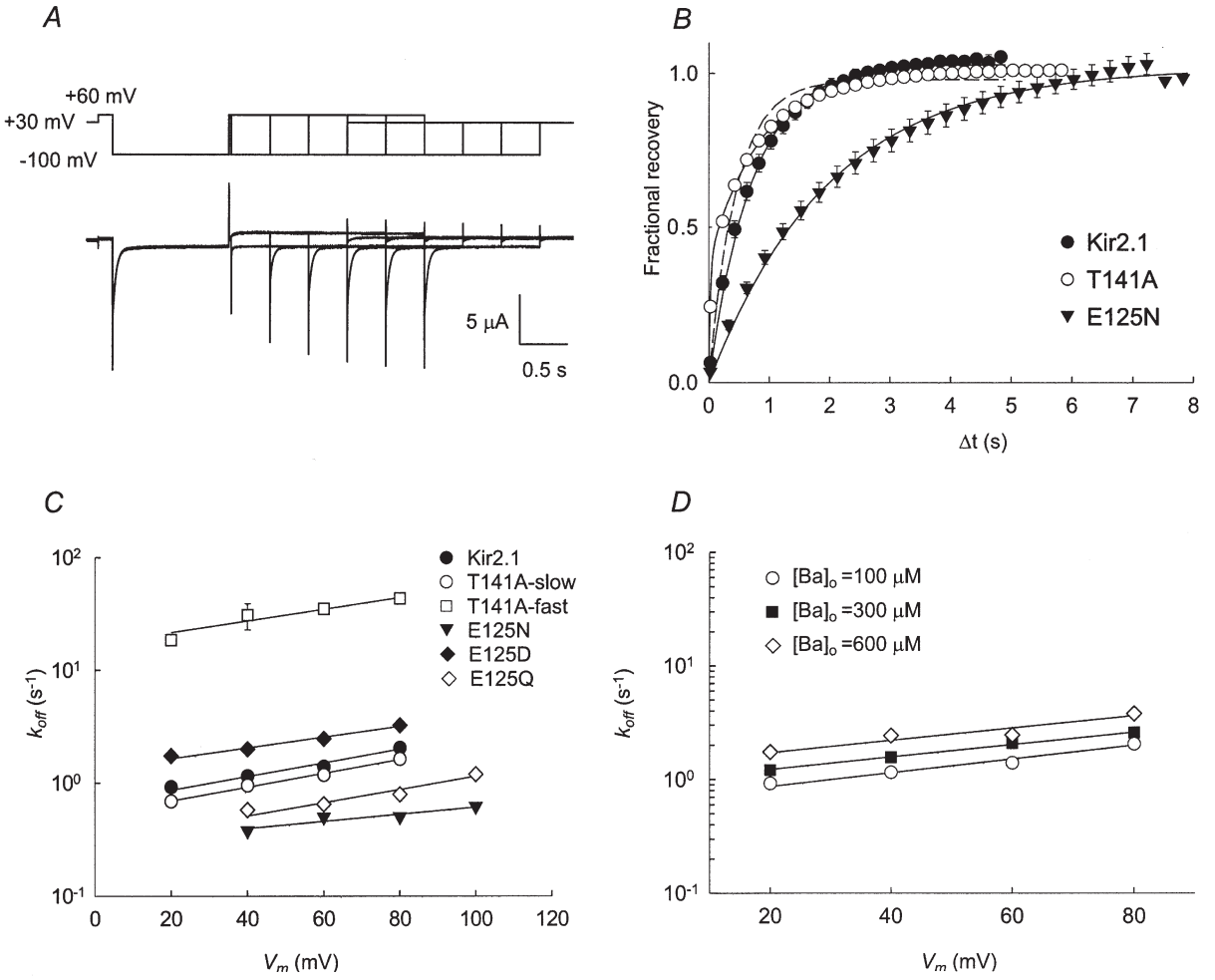

Figure 5. Recovery from Ba^{2+} block at positive potentials

A, illustration of the double pulse protocol used to measure recovery from block at +60 mV (top) and the associated Kir2.1 current traces (bottom). The current traces are superimposed. Channel block was initiated by a hyperpolarizing pulse to −100 mV for 1.2 s. *B*, time course of current recovery at +60 mV. In the case of Kir2.1 and Kir2.1(E125N) channels, the continuous lines are fits to eqn (8). In the case of Kir2.1(T141A), the data were fitted using eqn (8) (dashed line) and eqn (9) (continuous line). *C*, voltage dependence of the unblocking rate. The continuous lines are fits using eqn (10). *D*, recovery of Kir2.1 from the block at various external Ba^{2+} concentrations. The data points at $[Ba^{2+}]_o = 100\ \mu M$ are the same as in *C*.

Kir2.1(T141A): $k_{off,slow}(0) = 0.53 \pm 0.03\ s^{-1}$, $\delta_{off,slow} = 0.18 \pm 0.01$; and Kir2.1(T141A): $k_{off,fast}(0) = 17.11 \pm 2.71\ s^{-1}$, $\delta_{off,fast} = 0.15 \pm 0.03$. The rate of current recovery was independent of the extracellular Ba^{2+} concentration. This is evidenced by the fact that repeating the measurements at higher external Ba^{2+} concentrations (300 μM and 600 μM for Kir2.1 and 1 mM for Kir2.1(T141A) and Kir2.1(E125N) channels) yielded essentially the same results: for Kir2.1, $k_{off}(0) = 0.66\ s^{-1}$, $\delta_{off} = 0.18$ at $[Ba^{2+}]_o = 100\ \mu$M; $k_{off}(0) = 0.96\ s^{-1}$, $\delta_{off} = 0.16$ at $[Ba^{2+}]_o = 300\ \mu$M; $k_{off}(0) = 1.34\ s^{-1}$, $\delta_{off} = 0.16$ at $[Ba^{2+}]_o = 600\ \mu$M (Fig. 5*D*). These results suggest that at the voltages measured, the apparent rates of current recovery mainly reflect the unblocking rate, with only a negligible contribution from the blocking process.

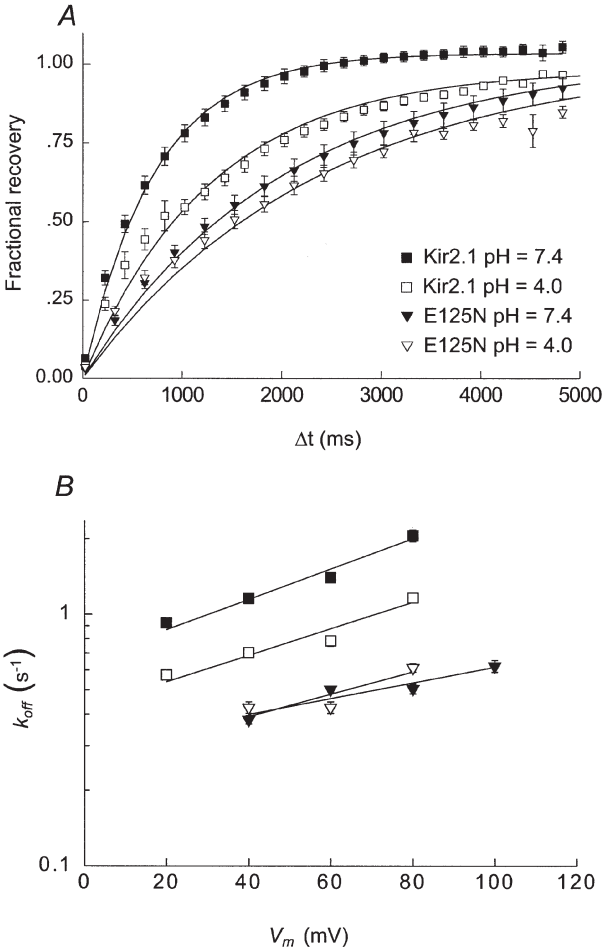

Figure 6. Effect of lowering the extracellular pH on the unblocking rates in Kir2.1 and Kir2.1(E125N) at positive potentials

A, time course for current recovery at +60 mV in external solutions at either pH 7.4 (filled symbols) or pH 4.0 (open symbols) for the Kir2.1 (squares) and Kir2.1(E125N) (triangles) channels. The continuous lines are fits to eqn (8). *B*, voltage dependence of the unblocking rates. The data points at pH 7.4 are the same as in Fig. 5*C*. The continuous lines are fits to eqn (10).

Effect of different amino acid residues on unblocking rates

The E125N mutation caused a large decrease in the rate of unblocking. To see whether this effect is due to the lack of negative charge or, rather, to the change in side-chain length, two more mutants were generated: Kir2.1(E125D), in which the negative charge is conserved and Kir2.1(E125Q), which lacks a negative charge at the 125 position. We first established the steady-state blocking properties of these two mutants. For Kir2.1(E125D): $K_d(-80) = 0.7 \pm 0.02\ \mu$M, $K_d(0) = 28 \pm 1\ \mu$M, $\delta = 0.6 \pm 0.01$. For Kir2.1(E125Q): $K_d(-80) = 7 \pm 0.4\ \mu$M, $K_d(0) = 194 \pm 3\ \mu$M, $\delta = 0.55 \pm 0.04$. These results argue that the negative charge at the 125 position plays a major role in Ba^{2+} blocking at steady state. Interestingly, the E125Q mutation did not reduce the voltage dependence of blocking. Next, the effect of these two mutations on the rate of recovery from Ba^{2+} block was measured. At +60 mV, Kir2.1(E125D) displayed an increased unblocking rate compared to the wild-type: $k_{off} = 2.47 \pm 0.09\ s^{-1}$ ($\tau_{recovery} = 0.4 \pm 0.01$ s). The unblocking rate of Kir2.1(E125Q) was similar to that of Kir2.1(E125N): $k_{off} = 0.65 \pm 0.02\ s^{-1}$ ($\tau_{recovery} = 1.54 \pm 0.04$ s). For both mutants, the voltage dependence of unblocking was similar to that of Kir2.1, with $\delta_{off} = 0.14 \pm 0.01$ for Kir2.1(E125D) and $\delta_{off} = 0.17 \pm 0.03$ for Kir2.1(E125Q). These results suggest that it is the negative charge at the 125 position, rather than side-chain length, which is responsible for speeding the rate of recovery from Ba^{2+} block.

The effect of extracellular acidification on unblocking rates

It is evident that the unblocking rates of Ba^{2+} ions are greatly affected by the presence of a negative charge at the 125 position. The possibility still exists that the E125N mutation induced a major structural perturbation that affected the pore indirectly. To directly show that the presence of the negative charge at the 125 position plays a role in speeding the unblocking rate of Ba^{2+} ions, we measured the unblocking rates of Ba^{2+} ions at pH 4 (which is close to the pK_a of the carboxylic side-chain of glutamate, 4.3) at various positive potentials. At +60 mV, the unblocking rate of Kir2.1 was significantly reduced from $1.40 \pm 0.03\ s^{-1}$ at pH 7.4 to $0.78 \pm 0.04\ s^{-1}$ at pH 4. In contrast, the unblocking rate of Kir2.1(E125N) was not affected by the acidic solution, with $k_{off} = 0.50 \pm 0.01\ s^{-1}$ at pH 7.4 compared to $k_{off} = 0.43 \pm 0.02\ s^{-1}$ at pH 4 (Fig. 6*A*). The voltage dependence of the unblocking rates was similar for the Kir2.1 and Kir2.1(E125N) channels in both solutions (Fig. 6*B*). These results suggest that the reduction in unblocking rate at acidic pH is mainly due to the titration of the carboxylic side-chain of the glutamate at position 125.

Effect of extracellular K^+ on the unblocking kinetics

Neyton & Miller (1988*a*,*b*) showed that up to three K^+ ions and one Ba^{2+} ion can bind in single file inside the BK (large conductance calcium-activated K^+) channel pore.

Binding of K^+ ions to a 'lock in' site extracellular to the blocking site impeded the exit of blocking Ba^{2+} ions towards the extracellular side. The same phenomenon was demonstrated in *Shaker*, a voltage-gated channel (Harris *et al.* 1998). To examine whether the existence of a similar site may account for the slower blocking and unblocking rates exhibited by Kir2.1(E125N), the unblocking experiment was repeated with 10 mM external K^+ ions. The unblocking rates measured under these conditions were essentially identical to the ones measured in 90K solution (data not shown). This result does not completely rule out a role of E125 in K^+ binding, as the site might already be saturated at 10 mM KCl. Performing the experiment at extracellular K^+ concentrations lower than 10 mM KCl was technically impractical, due to the limitations on acceptable channel expression levels (see Methods).

Single-channel conductance properties

Our results show that the amino acids at positions 125 and 141 of Kir2.1 control the rate at which Ba^{2+} ions enter and leave the pore. To examine whether E125N and T141A have a similar effect on K^+ permeation, single-channel currents were recorded from Kir2.1 and the two mutant channels (Fig. 7). Both Kir2.1(E125N) and Kir2.1(T141A) displayed reduced single-channel conductance relative to Kir2.1: 17 pS for Kir2.1(E125N) and 19 pS for Kir2.1(T141A), compared to 22 pS for Kir2.1 (Fig. 7). Addition of Ba^{2+} to the patch pipette did not affect the single-channel conductance, but increased the closed/blocked durations (results not shown).

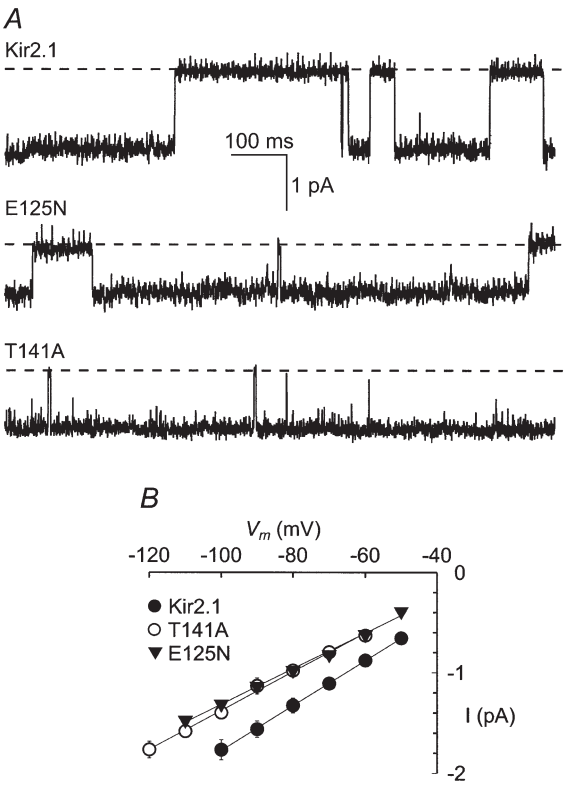

Figure 7. Single-channel recordings of Kir2.1, Kir2.1(E125N) and Kir2.1(T141A) channels

A, single-channel currents of oocytes expressing Kir2.1 (top), Kir2.1(E125N) (middle) and Kir2.1(T141A) (bottom) channels. The currents were recorded from cell-attached patches at −80 mV. The dashed lines denote closed channel current levels. *B*, current *vs.* voltage plot of the single-channel current amplitudes. The continuous lines are linear regressions.

The properties of the double mutant Kir2.1(E125N–T141A)

Our results demonstrate a unique and distinct role for the amino acids at positions 125 and 141 in aiding Ba^{2+} interactions with the channel. To further prove that these roles are distinct and independent, we generated the double mutant Kir2.1(E125N–T141A), and measured steady-state block. The degree of coupling between these two sites on the Kir2.1 protein is given by:

$$\Omega = \frac{K_d(\mathrm{WT,WT}) \times K_d(\mathrm{E125N–T141A})}{K_d(\mathrm{E125N}) \times K_d(\mathrm{T141A})}, \qquad (11)$$

(Horovitz & Fersht, 1990; Serrano *et al.* 1990; Hidalgo & MacKinnon, 1995; Imredy & MacKinnon, 2000). At −80 mV the equation yielded $\Omega = 0.45 \pm 0.13$, a value that deviates only slightly from unity, indicating that the 125 and 141 sites are not energetically coupled.

DISCUSSION

Barium block of Kir2.1 channels is affected by two distinct residues, a glutamic acid at position 125 located in the channel external vestibule and a threonine at position 141 located within the channel pore. The two residues have different effects on the blocking kinetics of the channel. Removing the negative charge at position 125 greatly affects Ba^{2+} blocking and unblocking rates as well as K^+ permeation. In contrast, replacing the theronine at position 141 with alanine reduced the affinity of Ba^{2+} for its binding site, without affecting its exit rate. These observations suggest a specific and unique role for each of these residues in the mechanism of Kir2.1 channel block by Ba^{2+} ions. A plausible mechanism and its possible implications for potassium ion permeation are discussed below.

To illustrate the mechanism of Ba^{2+} block of the Kir2.1 channel, we have used the blocking rate constant at 0 mV, $k_{on}(0)$, and the Eyring rate theory (Hille, 1992) to estimate the energy barrier for Ba^{2+} binding at zero membrane potential (Fig. 8*A*). According to the Eyring rate theory, the blocking rate k_{on} is related to the difference between the Gibbs free energy of the state in which the ion enters the channel (which is set to be 0 at 1 M concentration), and the barrier height, ΔG_{on}. This theory is described by the following equation:

$$k_{on} = \upsilon \exp(\Delta G_{on}/RT), \qquad (12)$$

where υ is the oscillation frequency, and R and T have their conventional meanings. The value of $10^9\ s^{-1}$ was assigned to υ, as was previously used in describing the Mg^{2+} block of Ca^{2+} and NMDA channels (Kuo & Hess, 1993*b*; Li-Smerin & Johnson, 1996). The depth of the energy well, $\Delta G°$ was calculated for zero membrane potential using:

$$\Delta G° = RT\ln K_d. \quad (13)$$

The barrier–well energy profile calculated for Kir2.1 and the mutants is consistent with E125N raising the energy barrier for Ba^{2+} entry, and T141A raising the barrier and, in addition, making the well less deep (Fig. 8*A*).

The E125N mutation reduced the voltage dependence of the steady-state Ba^{2+} block compared to the Kir2.1, Kir2.1(E125D), Kir(E125Q) and Kir2.1(T141A) channels. Two possibilities exist to explain this difference. The first is that the mutation affects channel structure in such a way that the Ba^{2+} ion experiences a different electric field. Our data do not support this possibility, as the voltage dependence of the blocking and unblocking rates was similar between Kir2.1(E125N), Kir2.1(E125Q) and Kir2.1 channels (at voltages more positive than −100 mV). The second possibility is that the Kir2.1(E125N) mutant channel allows Ba^{2+} permeation. Ba^{2+} permeation was shown to occur in other K^+ channels and was suggested to occur in Kir channels under high driving forces (see Results). Indeed, a monotonic increase in k_{off} can be seen for the Kir2.1(E125N) channel mutant over the whole voltage range and was more pronounced at potentials more hyperpolarized than −90 mV (Fig. 4*C*). This suggests that Ba^{2+} ions can permeate the Kir2.1(E125N) channel at all voltages tested. Ba^{2+} permeation in Kir2.1(E125N) is not due to the lack of negative charge at this position because the Kir2.1(E125Q) mutant channel does not display this characteristic, suggesting that the combination of a short side-chain and the lack of the negative charge at this position is required. The structural implication of this mutation on channel permeation properties is not yet established. Nevertheless, the ability of the Kir2.1(E125N) channel mutant to allow Ba^{2+} permeation at steady state may result in an over-estimation of the dissociation constant, leading to an under-estimation of the voltage dependence of the steady-state block.

Neyton & Miller (1988*b*) and later Harris *et al.* (1998) showed that BK and *Shaker* channels possess three discrete K^+-binding sites: a 'lock-in', an 'enhancement' and a 'deep high-affinity' site. These sites respectively impede the exit of the Ba^{2+} ion in the outward direction at low K^+ concentrations, enhance the exit of Ba^{2+} in the inward direction in the presence of high K^+ concentrations, and show high-affinity deep binding inside the pore. We initially hypothesized that the glutamate at position 125 may form part of the lock in site in Kir2.1. To test this, we lowered the extracellular K^+ concentration to 10 mM (further reduction in the concentration of external K^+ was impractical because inward currents became too small). In the presence of an almost 10-fold reduction in extracellular K^+ concentration, the unblocking of Ba^{2+} was unaffected in both the wild-type and Kir2.1(E125N)

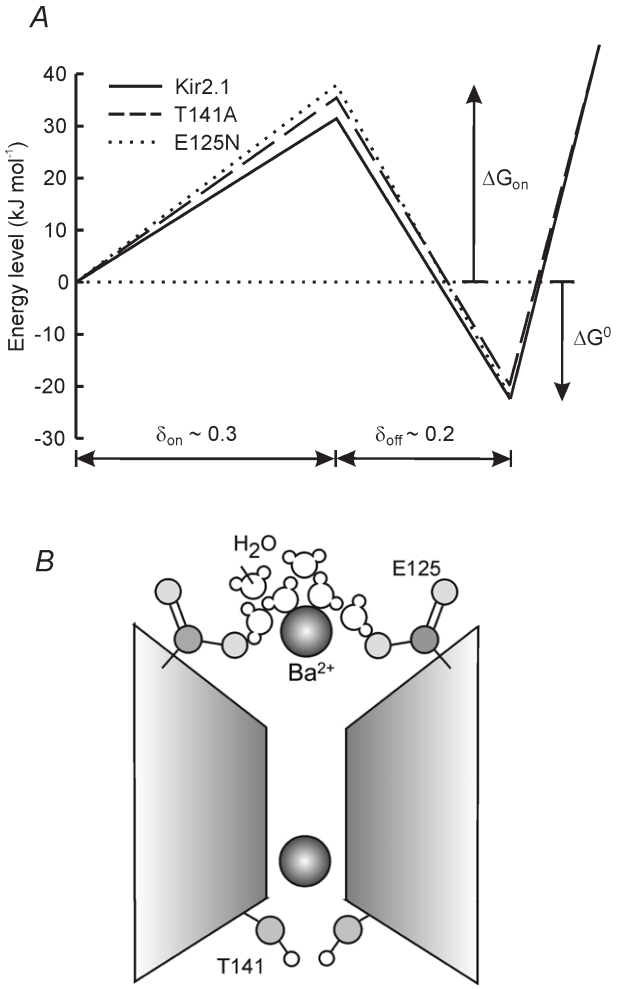

Figure 8. Energetic profile of Ba^{2+} blocking interaction with the Kir2.1 pore

A, energy profile for Ba^{2+} binding to the Kir2.1 channel and the two mutants Kir2.1(T141A) and Kir(E125N). The ΔG_{on} values were calculated from the blocking rates at 0 mV using the Eyring rate theory model (see Discussion): 31.4 kJ mol^{-1} for Kir2.1 (continuous line), 35.6 kJ mol^{-1} for Kir2.1(T141A) (dashed line) and 37.7 kJ mol^{-1} for Kir2.1(E125N) (dotted line). The $\Delta G°$ values were calculated from the steady-state dissociation constants (K_d) at 0 mV (see Discussion): −22.6 kJ mol^{-1} for Kir2.1, −19.7 kJ mol^{-1} for Kir2.1(T141A) and −22.2 kJ mol^{-1} for Kir2.1(E125N). *B*, a cartoon model describing the role of E125 and T141 residues in barium block. The negatively charged E125 side-chain presumably participates in the interaction with the Ba^{2+} ion and its associated water molecules. The polar hydroxyl group (light grey) of T141 stabilizes the interaction of the blocking ion with its binding site.

channels. If the lock in site is indeed affected by the glutamate at position 125 we would expect to see a change in the exit rate of Ba^{2+} from the pore. The inability to record a difference in 10 mM K^+ may suggest either that the lock in site in Kir2.1 has a higher than 10 mM affinity for K^+ ions, and/or that a lock in site is not affected by the glutamate side-chain at position 125 in Kir2.1. Since a mutation at this site affects the rate at which K^+ ions permeate the channel (Fig. 7), and K^+ saturates the pore at rather low concentrations (Shieh *et al.* 1999), we suggest that the glutamate at position 125 is involved in K^+ permeation and may be forming the initial entry site to the long pore that possesses multiple binding sites for K^+ ions (Fig. 8*B*; Hille & Schwarz, 1978).

It is possible that the increase in the barrier for Ba^{2+} exit and entry exhibited in Kir2.1(E125N) may be linked to hydration and dehydration processes. Dehydration is a required step before a blocking Ba^{2+} ion or permeating K^+ ions can enter the narrow part of the pore (selectivity filter). It is possible that the negative charge at position 125 helps to coordinate this process. The 4-fold symmetry of Kir2.1 channels may cause the formation of a negatively charged ring at the pore entrance. Approaching Ba^{2+} ions (as well as permeating K^+ ions) may be stripped of their hydration cloud more efficiently as a result of the interaction with the negatively charged ring, thus leading to enhanced flux rates (Fig. 8*B*). However, it is not obligatory for Kir channels to possess such a mechanism to allow efficient K^+ permeation, as some Kir channels do not carry a negative charge at this position. An alternative explanation for the role of the glutamate at position 125 may be to contribute to the attraction forces between the positively charged permeating ion and the channel pore vestibule. These forces may help to reorient the permeating ion towards the pore and thus to increase the probability of a K^+ ion entering the pore. The involvement of external carboxylic residues in ion entry and selectivity has been shown in other cationic channels, such as voltage-gated calcium and sodium channels (Hille, 1975; Kuo & Hess, 1993*a*; Yang *et al.* 1993; French *et al.* 1994; Ellinor *et al.* 1995). This may suggest a rather general mechanism for the initial interaction of cations with cation channels.

The T141A mutation reduced the overall affinity for Ba^{2+} by destabilizing the binding site, as the $\Delta G°$ value is less negative in this mutant channel. The reduced energy of interaction for this mutant channel is not so profound as to abolish Ba^{2+} binding altogether. This suggests that T141 by itself is not solely creating the binding site. As T141 is located just two residues N-terminal to the selectivity filter (GYG), we speculate that the Ba^{2+} ion blocks Kir channels by binding within the selectivity filter, at a similar position to the deeper K^+-binding site (Doyle *et al.* 1998), and that the T141 side-chain stabilizes this interaction (Fig. 8*B*). This suggestion has been recently supported by the work of Jiang & MacKinnon (2000), who obtained the crystal structure of the KcsA channel with a bound Ba^{2+} ion. The Ba^{2+} ion was found to be bound to the intracellular end of the selectivity filter, very close indeed to the residue corresponding to T141. Another piece of evidence supporting this suggestion comes from the work of Lu *et al.* (2001), in which unnatural backbone changes from an amide carbonyl to an ester bond were introduced into the selectivity filter of Kir2.1. Remarkably, this change left the selectivity of the channel intact, but profoundly affected the affinity to deep channel blockers such as Cs^+ and Ba^{2+} ions.

At the level of their primary structure, most potassium channels display a similar sequence underlying their selective permeation for potassium ions (Heginbotham *et al.* 1992; Lu & Miller, 1995; Pascual *et al.* 1995; Dart *et al.* 1998; Doyle *et al.* 1998). In *Shaker* K^+ channels, residues in the signature sequence and around it have been found to affect block by external Ba^{2+} ions (Hurst *et al.* 1996; Harris *et al.* 1998). Notably, the threonine at position 441 in *Shaker*, which is located at the corresponding position to T141 in Kir2.1, also affected the affinity for Ba^{2+} block. However, in the *Shaker* channel, the mutation T441C increased the unblocking rate of Ba^{2+} from its deep binding site (Harris *et al.* 1998), whereas in Kir2.1 the mutation T141A did not change the unblocking rate. Scanning cysteine accessibility mutagenesis experiments on Kir2.1 showed that T141C renders the channel sensitive to Ag^+ ions, suggesting that the T141 side-chain points towards the permeation pathway (Dart *et al.* 1998). In contrast, in the *Shaker* channel, the T441C residue was inaccessible to Ag^+ ions (Lu & Miller, 1995). There may be slight variations in the role T141 plays in Ba^{2+} block even within the Kir channel family: it was shown that in Kir1.2 the V121T mutation, in the site that corresponds to T141 in Kir2.1, affects both the blocking and unblocking rates of Ba^{2+} (Zhou *et al.* 1996). Taken together, these pieces of evidence suggest that the T141 side-chain may adopt a different orientation in different K^+ channels, and thus play slightly different roles in the coordinated binding of the Ba^{2+} ion. Since the T141 residue actively participates in K^+ conduction in addition to Ba^{2+} binding (Choe *et al.* 2000), it may play a different role in K^+ permeation as well. Since the recent elucidation of the crystal structure of KcsA (Doyle *et al.* 1998), evidence has been gathering to suggest that that the overall three-dimensional structure of the pore of the Kir2.1 channel may be slightly different from the one found in KcsA (Dart *et al.* 1998; Thompson *et al.* 2000). It is then rather intriguing to think that despite the high similarity in their primary structure, different K^+ channels may possess slightly different mechanisms for K^+-selective permeation.

In summary, we have identified two distinct mechanisms that affect Ba^{2+} block of Kir2.1 channels. These two mechanisms influence either the entry or the stability of Ba^{2+} within the pore. The E125 residue participates in

assisting the entry of Ba^{2+} into the pore, whereas the T141 residue is involved in the stabilization of the Ba^{2+} ion in its deep binding site.

Biermans, G., Vereecke, J. & Carmeliet, E. (1987). The mechanism of the inactivation of the inward-rectifying K current during hyperpolarizing steps in guinea-pig ventricular myocytes. *Pflügers Archiv* **410**, 604–613.

Carmeliet, E. & Mubagwa, K. (1986). Characterization of the acetylcholine-induced potassium current in rabbit cardiac Purkinje fibres. *Journal of Physiology* **371**, 219–237.

Choe, H., Sackin, H. & Palmer, L. G. (2000). Permeation properties of inward-rectifier potassium channels and their molecular determinants. *Journal of General Physiology* **115**, 391–404.

Dart, C., Leyland, M. L., Spencer, P. J., Stanfield, P. R. & Sutcliffe, M. J. (1998). The selectivity filter of a potassium channel, murine Kir2.1, investigated using scanning cysteine mutagenesis. *Journal of Physiology* **511**, 25–32.

Doring, F., Derst, C., Wischmeyer, E., Karschin, C., Schneggenburger, R., Daut, J. & Karschin, A. (1998). The epithelial inward rectifier channel Kir7.1 displays unusual K^+ permeation properties. *Journal of Neuroscience* **18**, 8625–8636.

Doyle, D. A., Cabral, J. M., Pfuetzner, R. A., Kuo, A., Gulbis, J. M., Cohen, S. L., Chait, B. T. & MacKinnon, R. (1998). The structure of the potassium channel: molecular basis of K^+ conduction and selectivity. *Science* **280**, 69–77.

Ellinor, P. T., Yang, J., Sather, W. A., Zhang, J. F. & Tsien, R. W. (1995). Ca^{2+} channel selectivity at a single locus for high-affinity Ca^{2+} interactions. *Neuron* **15**, 1121–1132.

Fakler, B., Brandle, U., Glowatzki, E., Weidemann, S., Zenner, H. P. & Ruppersberg, J. P. (1995). Strong voltage-dependent inward rectification of inward rectifier K^+ channels is caused by intracellular spermine. *Cell* **80**, 149–154.

French, R. J., Worley, J. F. III, Wonderlin, W. F., Kularatna, A. S. & Krueger, B. K. (1994). Ion permeation, divalent ion block, and chemical modification of single sodium channels. Description by single- and double-occupancy rate-theory models. *Journal of General Physiology* **103**, 447–470.

Grigoriev, N. G., Spafford, J. D. & Spencer, A. N. (1999). The effects of level of expression of a jellyfish *Shaker* potassium channel: a positive potassium feedback mechanism. *Journal of Physiology* **517**, 25–33.

Hamill, O. P., Marty, A., Neher, E., Sakmann, B. & Sigworth, F. J. (1981). Improved patch-clamp techniques for high-resolution current recording from cells and cell-free membrane patches. *Pflügers Archiv* **391**, 85–100.

Harris, R. E., Larsson, H. P. & Isacoff, E. Y. (1998). A permanent ion binding site located between two gates of the Shaker K^+ channel. *Biophysical Journal* **74**, 1808–1820.

Harvey, R. D. & Ten Eick, R. E. (1989). Voltage-dependent block of cardiac inward-rectifying potassium current by monovalent cations. *Journal of General Physiology* **94**, 349–361.

Heginbotham, L., Abramson, T. & MacKinnon, R. (1992). A functional connection between the pores of distantly related ion channels as revealed by mutant K^+ channels. *Science* **258**, 1152–1155.

Hidalgo, P. & MacKinnon, R. (1995). Revealing the architecture of a K^+ channel pore through mutant cycles with a peptide inhibitor. *Science* **268**, 307–310.

Hille, B. (1975). Ionic selectivity, saturation, and block in sodium channels. A four- barrier model. *Journal of General Physiology* **66**, 535–560.

Hille, B. (1992). *Ionic Channels of Excitable Membranes*. Sinauer Assoc., Sunderland, MA.

Hille, B. & Schwarz, W. (1978). Potassium channels as multi-ion single file pores. *Journal of General Physiology* **72**, 409–442.

Honore, E., Attali, B., Romey, G., Lesage, F., Barhanin, J. & Lazdunski, M. (1992). Different types of K^+ channel current are generated by different levels of a single mRNA. *EMBO Journal* **11**, 2465–2471.

Horovitz, A. & Fersht, A. R. (1990). Strategy for analysing the co-operativity of intramolecular interactions in peptides and proteins. *Journal of Molecular Biology* **214**, 613–617.

Hurst, R. S., Toro, L. & Stefani, E. (1996). Molecular determinants of external barium block in Shaker potassium channels. *FEBS Letters* **388**, 59–65.

Imredy, J. P. & MacKinnon, R. (2000). Energetic and structural interactions between delta-dendrotoxin and a voltage-gated potassium channel. *Journal of Molecular Biology* **296**, 1283–1294.

Jiang, Y. & MacKinnon, R. (2000). The barium site in a potassium channel by x-ray crystallography. *Journal of General Physiology* **115**, 269–272.

Krapivinsky, G., Medina, I., Eng, L., Krapivinsky, L., Yang, Y,. & Clapham, D. E. (1998). A novel inward rectifier K^+ channel with unique pore properties. *Neuron* **20**, 995–1005.

Kubo, Y., Baldwin, T. J., Jan, Y. N. & Jan, L. Y. (1993). Primary structure and functional expression of a mouse inward rectifier potassium channel. *Nature* **362**, 127–133.

Kuo, C. C. & Hess, P. (1993*a*). Characterization of the high-affinity Ca^{2+} binding sites in the L-type Ca^{2+} channel pore in rat phaeochromocytoma cells. *Journal of Physiology* **466**, 657–682.

Kuo, C. C. & Hess, P. (1993*b*). Block of the L-type Ca^{2+} channel pore by external and internal Mg^{2+} in rat phaeochromocytoma cells. *Journal of Physiology* **466**, 683–706.

Li-Smerin, Y. & Johnson, J. W. (1996). Kinetics of the block by intracellular Mg^{2+} of the NMDA-activated channel in cultured rat neurons. *Journal of Physiology* **491**, 121–135.

Lopatin, A. N., Makhina, E. N. & Nichols, C. G. (1995). The mechanism of inward rectification of potassium channels: "long-pore plugging" by cytoplasmic polyamines. *Journal of General Physiology* **106**, 923–955.

Lu, T., Ting, A. Y., Jan, L. Y., Schultz, P. G. & Yang, J. (2001) Probing ion permeation and gating in a K^+ channel with backbone mutations in the selectivity filter. *Nature Neuroscience* **4**, 239–246.

Lu, Q. & Miller, C. (1995). Silver as a probe of pore-forming residues in a potassium channel. *Science* **268**, 304–307.

Moran, O., Schreibmayer, W., Weigl, L., Dascal, N. & Lotan, I. (1992). Level of expression controls modes of gating of a K^+ channel. *FEBS Letters* **302**, 21–25.

Navaratnam, D. S., Escobar, L., Covarrubias, M. & Oberholtzer, J. C. (1995). Permeation properties and differential expression across the auditory receptor epithelium of an inward rectifier K^+ channel cloned from the chick inner ear. *Journal of Biological Chemistry* **270**, 19238–19245.

Neyton, J. & Miller, C. (1988*a*). Potassium blocks barium permeation through a calcium-activated potassium channel. *Journal of General Physiology* **92**, 549–567.

Neyton, J. & Miller, C. (1988*b*). Discrete Ba^{2+} block as a probe of ion occupancy and pore structure in the high-conductance Ca^{2+}-activated K^+ channel. *Journal of General Physiology* **92**, 569–586.

Ohmori, H. (1978). Inactivation kinetics and steady-state current noise in the anomalous rectifier of tunicate egg cell membranes. *Journal of Physiology* **281**, 77–99.

Pascual, J. M., Shieh, C. C., Kirsch, G. E. & Brown, A. M. (1995). K^+ pore structure revealed by reporter cysteines at inner and outer surfaces. *Neuron* **14**, 1055–1063.

Reuveny, E., Jan, Y. N. & Jan, L. Y. (1996). Contributions of a negatively charged residue in the hydrophobic domain of the Kir2.1 inwardly rectifying K^+ channel to $K(^+)$-selective permeation. *Biophysical Journal* **70**, 754–761.

Sabirov, R. Z., Okada, Y. & Oiki, S. (1997*a*). Two-sided action of protons on an inward rectifier K^+ channel (Kir2.1). *Pflügers Archiv* **433**, 428–434.

Sabirov, R. Z., Tominaga, T., Miwa, A., Okada, Y. & Oiki, S. (1997*b*). A conserved arginine residue in the pore region of an inward rectifier K channel (IRK1) as an external barrier for cationic blockers. *Journal of General Physiology* **110**, 665–677.

Serrano, L., Horovitz, A., Avron, B., Bycroft, M. & Fersht, A. R. (1990). Estimating the contribution of engineered surface electrostatic interactions to protein stability by using double-mutant cycles, *Biochemistry* **29**, 9343–9352.

Shieh, R. C., Chang, J. C. & Arreola, J. (1998). Interaction of Ba^{2+} with the pores of the cloned inward rectifier K^+ channel Kir2.1 expressed in *Xenopus* oocytes. *Biophysical Journal* **75**, 2313–2322.

Shieh, R. C., Chang, J. C. & Kuo, C. C. (1999). K^+ binding sites and interactions between permeating K^+ ions at the external pore mouth of an inward rectifier K^+ channel (Kir2.1). *Journal of Biological Chemistry* **274**, 17424–17430.

Shioya, T., Matsuda, H. & Noma, A. (1993). Fast and slow blockades of the inward-rectifier K^+ channel by external divalent cations in guinea-pig cardiac myocytes. *Pflügers Archiv* **422**, 427–435.

Standen, N. B. & Stanfield, P. R. (1978). A potential- and time-dependent blockade of inward rectification in frog skeletal muscle fibres by barium and strontium ions. *Journal of Physiology* **280**, 169–191.

Standen, N. B. & Stanfield, P. R. (1980). Rubidium block and rubidium permeability of the inward rectifier of frog skeletal muscle fibres. *Journal of Physiology* **304**, 415–435.

Thompson, G. A., Leyland, M. L., Ashmole, I., Sutcliffe, M. J. & Stanfield, P. R. (2000). Residues beyond the selectivity filter of the K^+ channel Kir2.1 regulate permeation and block by external Rb^+ and Cs^+. *Journal of Physiology* **526**, 231–240.

Topert, C., Doring, F., Wischmeyer, E., Karschin, C., Brockhaus, J., Ballanyi, K., Derst, C. & Karschin, A. (1998). Kir2.4: a novel K^+ inward rectifier channel associated with motoneurons of cranial nerve nuclei. *Journal of Neuroscience* **18**, 4096–4105.

Woodhull, A. M. (1973). Ionic blockage of sodium channels in nerve. *Journal of General Physiology* **61**, 687–708.

Yang, J., Ellinor, P. T., Sather, W. A., Zhang, J. F. & Tsien, R. W. (1993). Molecular determinants of Ca^{2+} selectivity and ion permeation in L-type Ca^{2+} channels. *Nature* **366**, 158–161.

Yang, X. C. & Sachs, F. (1989). Block of stretch-activated ion channels in *Xenopus* oocytes by gadolinium and calcium ions. *Science* **243**, 1068–1071.

Zhang, Y., McBride, D. W. Jr & Hamill, O. P. (1998). The ion selectivity of a membrane conductance inactivated by extracellular calcium in *Xenopus* oocytes. *Journal of Physiology* **508**, 763–776.

Zhou, H., Chepilko, S., Schutt, W., Choe, H., Palmer, L. G. & Sackin, H. (1996). Mutations in the pore region of ROMK enhance Ba^{2+} block. *American Journal of Physiology* **271**, C1949–1956.

Acknowledgements

We would like to thank Dr Ziv Reich for helpful discussions, Dr Zeev Burshtein and Rona Sadja for critically reviewing the manuscript, and Ruth Meller and Elisha Shalgi for excellent technical assistance. This work was supported by the Israeli Science Foundation (Keren Dorot), The Minerva Foundation Germany, and the Human Frontier Science Program.

Corresponding author

E. Reuveny: Department of Biological Chemistry, Weizmann institute of Science, Rehovot 76100, Israel.

Email: e.reuveny@weizmann.ac.il